ARTICLE   OPEN

Check for updates

Superconducting dome by tuning through a van Hove singularity in a two-dimensional metal

Wen Wan [1], Rishav Harsh[1], Paul Dreher[1], Fernando de Juan [1,2] and Miguel M. Ugeda [1,2,3 ✉]

Chemical substitution is a promising route for the exploration of a rich variety of doping- and/or disorder-dependent collective phenomena in low-dimensional quantum materials. Here we show that transition metal dichalcogenide alloys are ideal platforms to this purpose. In particular, we demonstrate the emergence of superconductivity in the otherwise metallic single-layer $TaSe_2$ by minute electron doping provided by substitutional W atoms. We investigate the temperature and magnetic field dependence of the superconducting state of $Ta_{1-\delta}W_\delta Se_2$ with electron doping (δ) using variable temperature (0.34–4.2 K) scanning tunneling spectroscopy (STS). We unveil the emergence of a superconducting dome spanning $0.003 < \delta < 0.03$ with a maximized critical temperature of 0.9 K, a significant increase from that of bulk $TaSe_2$ ($T_C = 0.14$ K). Superconductivity emerges from an increase of the density of states (DOS) as the Fermi surface approaches a van Hove singularity due to doping. Once the singularity is reached, however, the DOS decreases with δ, which gradually weakens the superconducting state, thus shaping the superconducting dome. Lastly, our doping-dependent measurements suggest the development of a Coulomb glass phase triggered by disorder due to W dopants.

INTRODUCTION

The isolation and manipulation of atomically-thin crystals have recently enabled the investigation of wealth of exotic electronic phenomena. A remarkable example is the case of superconductivity (SC) in transition metal dichalcogenide (TMD) monolayers, where the strong spin-orbit coupling (SOC), together with the lack of inversion symmetry, triggers the emergence of unconventional superconducting properties such as the Ising pairing and symmetry-allowed triplet configurations[1–5]. Furthermore, most of the bulk TMD metal counterparts are superconducting, which enables interrogation of the effects of dimensionality and interlayer coupling. For example, the TMD metals 2H-MX_2 (M = Nb, Ta and X = S, Se) are intrinsic superconductors in bulk, but exhibit disparate behavior as they are thinned down to the monolayer. In NbX_2 monolayers, superconductivity shows significant weakening ($NbSe_2$)[6,7] and even disappearance (NbS_2)[8] with respect to bulk. In contrast, electron transport experiments in ultrathin films of TaX_2 (even reaching the monolayer in TaS_2) have revealed significant increase of the critical temperature (T_C)[9–13]. In $TaSe_2$, ionic-gating measurements revealed a substantial increase of $T_C = 1.4$ K of nm-thick films (~5 layers) as compared to the $T_C = 0.14$ K of bulk[10]. However, ultrathin films of TMD metals are highly susceptible to degradation in ambient conditions, which affects the intrinsic properties of collective electronic states (SC and CDW). Unfortunately, experimental work exploring the thickness dependence of SC in inert controlled environment is still scarce[6,12]. This leads to disparate qualities among the TMDs, which often make the results hardly comparable. Therefore, a coherent picture about the impact of dimensionality on the SC state has not yet been achieved for this family of layered materials.

In parallel to the exploration of the intrinsic ground state in correlated 2D systems, there has recently been an increasing interest in tuning their many-body electronic states. A successful approach here is the use of ionic gating, which has demonstrated

its effectiveness to reversibly manipulate the collective phases of 2D TMDs[14–16]. An alternative method to tune the electronic properties of a layered material is by chemical doping. However, this approach has been rarely used to manipulate many-body states[17,18], and most effort so far has focused on tuning the bandgap and mobility of TMD semiconductors[19–23]. Furthermore, chemical-doping strategies enable to interrogate the robustness and fundamental properties of many-body states in the presence of disorder, which remain largely unexplored due to the lack of suitable platforms.

In this work, we demonstrate that a monolayer of $TaSe_2$ does not hold superconductivity down to 340 mK (using samples unexposed to air) by using variable-temperature (0.34–4.2 K) scanning tunneling spectroscopy (STS). Furthermore, we induce superconductivity in this 2D material by electron doping using W atoms given the proximity of the Fermi level (E_F) to an empty van Hove singularity (vHs) in its DOS. First, our spatially resolved STS measurements confirm that W atoms are embedded in the $TaSe_2$ lattice acting as electron donors. We subsequently probe the low-energy electronic structure of lightly doped $TaSe_2$ monolayers and unveil the emergence of a superconducting dome on the temperature-doping phase diagram. Optimized superconductivity develops for a W concentration of 1.8% with $T_C \sim 0.9$ K, a significant increase from that of bulk ($T_C = 0.14$ K). The SC dome reflects the variations in the available electrons for pairing caused by the crossing of a vHs in the DOS spectrum, as the layer is electron doped. Lastly, we identify the formation of a Coulomb glass phase related to disorder and boosted by W dopants.

RESULTS AND DISCUSSION

Pristine monolayer $TaSe_2$

Our STM/STS experiments were carried out on $Ta_{1-\delta}W_\delta Se_2$ alloys in the dilute regime ($0 < \delta < 0.07$) grown on bilayer graphene (BLG)
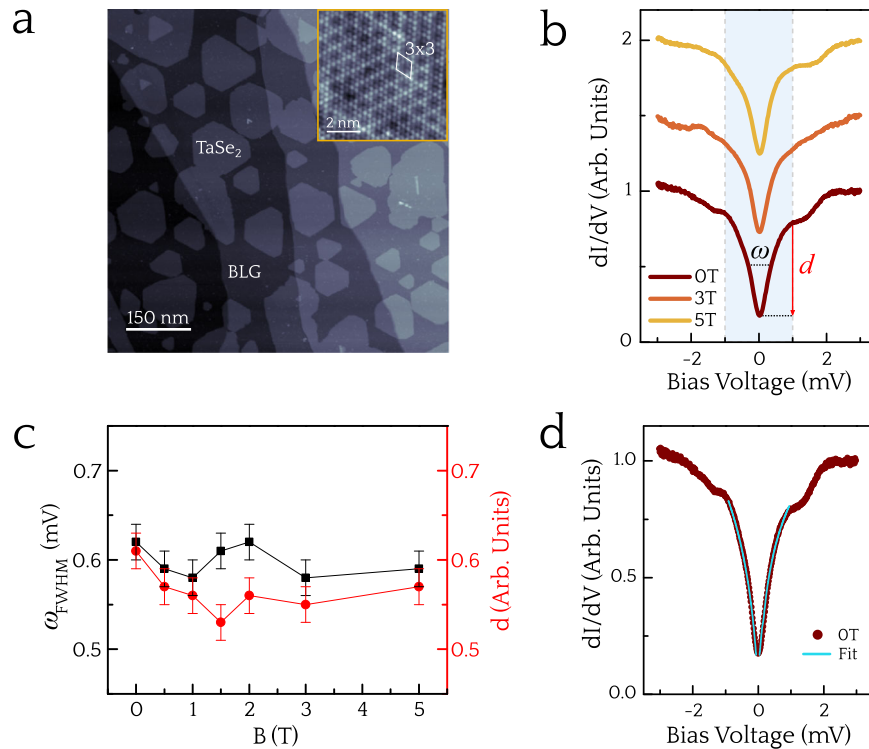
Fig. 1 Low-energy electronic structure of single-layer TaSe₂. a Large-scale STM image of monolayer TaSe₂/BLG ($V_s = 2$ V, $I = 20$ pA). Inset: STM image showing the 3×3 CDW ($V_t = 0.6$ V, $I = 100$ pA). **b** $B_\perp$-dependence of the electronic structure of monolayer TaSe₂ ($T = 0.34$ K). The shadowed region indicates the energy range of the inner dip. The width (ω) and depth (d) of this dip are defined with respect to the value at $dI/dV(1\,\text{mV})$). **c** The evolution of ω and d with $B_\perp$ in monolayer TaSe₂. The error bars represent the standard error of the mean. **d** $dI/dV(B_\perp = 0\,\text{T})$ on monolayer TaSe₂ (dots) and the DOS $\propto \text{Ln}(V)$ fit within ± 1 mV (line).

on 6H-SiC(0001) via molecular beam epitaxy (see "Methods"). We use graphene as a substrate since it plays a negligible role in the electronic structure of TMD monolayers, including the super-conductivity[24]. Single-layer TaSe₂ retains the characteristic 3×3 CDW order shown in bulk (see inset Fig. 1a), which induces a gap-like feature in the DOS of $2\triangle_{CDW} \approx 12$ meV around E_F (see Supplementary Information), in agreement with previous experiments[25]. First, we probe the existence of superconductivity in monolayer TaSe₂ ($\delta = 0$). Figure 1b shows the out-of-plane magnetic field ($B_\perp$) dependence of the low-energy electronic structure (± 3 meV) of the monolayer at $T = 0.34$ K. For $B = 0$ T, the differential conductance ($dI/dV \propto$ DOS) shows a pronounced dip in the DOS of width $\omega \sim 0.6$ meV at E_F which is, in principle, compatible with superconductivity. However, this dip is an electronic feature that remains unperturbed as $B_\perp$ is increased, as seen in the dI/dV spectra subsequently taken at $B = 3$ T and $B = 5$ T. To quantify this observation, we show the evolution of the width (ω) and depth of the dip (d) with $B_\perp$ in Fig. 1c. Both magnitudes remain roughly constant within our resolution (see Methods). In summary, the insensitivity of the dip with $B_\perp$ allows us to rule out the existence of superconductivity in monolayer TaSe₂ down to 0.34 K. The origin of the dip will be discussed later with additional disorder-dependent (W concentration) STS data.

The absence of superconductivity found in monolayer TaSe₂ is in contrast to transport experiments carried out in thin-films (multilayers) of TaSe₂, which report $T_C \sim 1$ K[9,10]. A plausible origin of these disparate results is the sensitivity of the SC state to oxidation as the TMD approaches the 2D limit as all the previous experiments used samples exposed to ambient conditions. Another possibility is that the superconductivity follows a non-monotonic evolution from bulk down to the monolayer limit. Although unlikely, we cannot exclude this possibility and,

therefore, detailed studies are required to fully understand the evolution of the superconductivity in TaSe₂. We emphasize, however, that the role of the BLG substrate in the super-conductivity is negligible, as we previously demonstrated by showing identical properties of single-layer NbSe₂ on BLG and h-BN[24]. The evolution of the superconductivity in TaSe₂ with crystal thickness departs from TaS₂, which undergoes a significant increase of T_C in the monolayer (3.5 K) with respect to the bulk (0.8 K).

Electron-doped TaSe₂

The absence of superconductivity in monolayer TaSe₂ raises the question whether electron doping could trigger its emergence. Electron-doping in TaSe₂ is expected to increase the available electrons at E_F to pair due to the proximity to a vHs in the DOS[26–28]. To this purpose, individual W atoms were embedded as substitutional atoms in the Ta plane during the layer growth. W has one more valence electron than Nb and, therefore, acts as electron donor (see Supplementary Information for the electronic characterization of the W dopants). The resulting monolayer is an aliovalent $Ta_{1-\delta}W_\delta Se_2$ alloy with a dilute W concentration (δ) that can be precisely characterized via STM imaging. As shown in Fig. 2, for W doping levels as low as 2.5% ($\delta = 0.025$) superconductivity develops. Figure 2a shows the evolution of the DOS in $Ta_{0.975}W_{0.025}Se_2$ with $B_\perp$ (see "Methods" for details on the $B_\perp$-dependent STS measurements). At zero field, the DOS also shows a similar dip centered at E_F. However, in contrast to the pristine TaSe₂ case (Fig. 1), this dip is now highly susceptible to $B_\perp$, and its depth gradually decreases as $B_\perp$ increases up to an upper critical field $B_{C_2} = 0.7$ T, a value beyond which the DOS remains unchanged (see Supplementary Information for the definition of critical values B_{C_2} and T_C). Furthermore, the dip now shows peaks
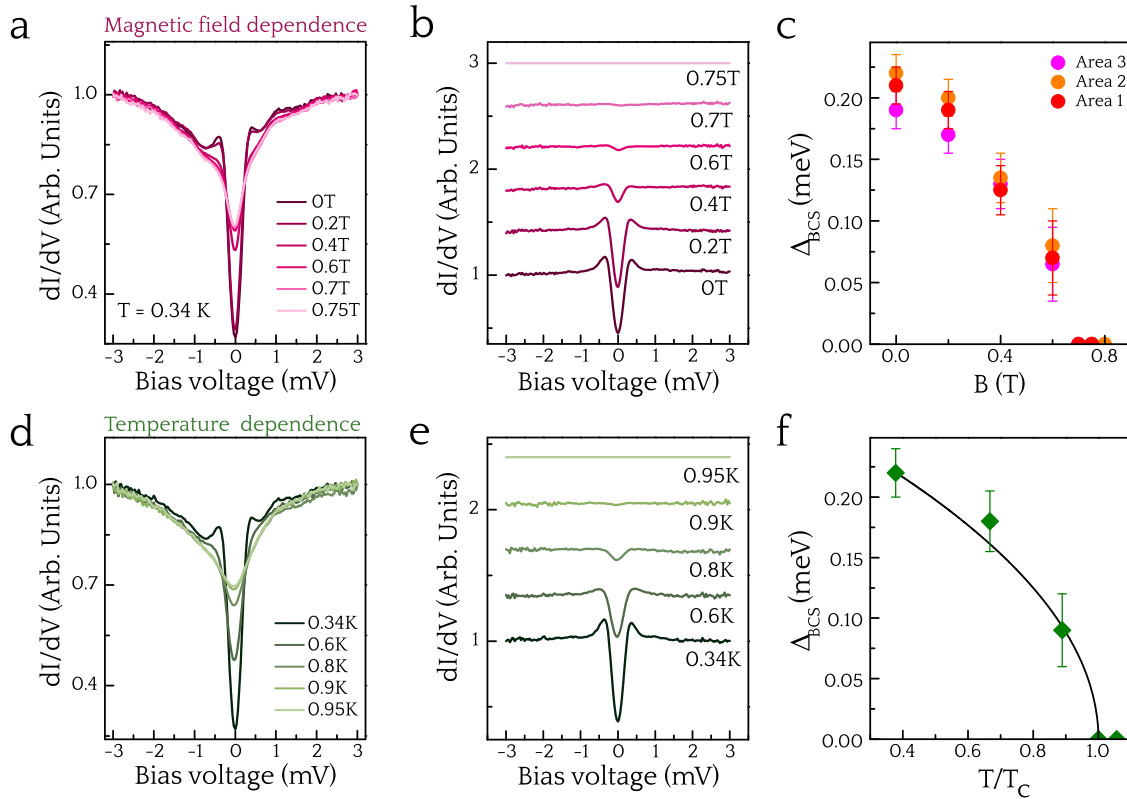
Fig. 2 Magnetic field and temperature dependence of the superconducting gap in electron-doped single-layer TaSe₂. **a** Magnetic field-dependence of the electronic structure of $Ta_{0.975}W_{0.025}Se_2$. **b** Same $dI/dV(B)$ spectra as in **a** normalized to $dI/dV(0.75\,T)$. **c** Evolution of the superconducting gap Δ_{BCS} with B measured in three different regions of the sample. The SC gap values have been extracted by fitting the normalized curves shown in **b**. **d** T-dependence of the electronic structure of $Ta_{0.975}W_{0.025}Se_2$. **e** Same $dI/dV(T)$ spectra as in **a** normalized to $dI/dV(0.95\,K)$. **f** BCS SC fit of the dip features observed after normalization in **e**. The line shows the expected BCS temperature dependence. The error bars in **c**, **f** show the standard error of the mean.

at its edges at $B = 0\,T$ that gradually disappear with $B_\perp$, which are consistent with superconducting coherence peaks. Figure 2b shows the set of $dI/dV(B_\perp)$ spectra of Fig. 2a normalized to $dI/dV(0.75\,T)$. As seen, a clear DOS dip centered at E_F evolves as $B_\perp$ is decreased. Since this sensitivity against $B_\perp$ is compatible with superconductivity, we fit these dI/dV spectra to a BCS gap Δ_{BCS} (see Supplementary Information for fitting details), and plot them as a function of $B_\perp$ (Fig. 2c, red dots). This figure shows the same measurements in another two regions of the same sample (pink and orange dots).

To confirm that the dip feature emerging in the normalized dI/dV spectra corresponds to a superconducting gap, we also study its temperature dependence in the same sample. Figure 2d show a series of dI/dV spectra acquired consecutively at different temperatures. Similarly, the dip with bound peaks decreases as the T increases up to 0.9 K, where it remains nearly unchanged. This evolution is better observed in the normalized spectra to $dI/dV(0.95\,K)$ in Fig. 2e. We fit the normalized $dI/dV(T)$ spectra to a SC gap following the same procedure, and Fig. 2f shows the evolution of Δ_{BCS} with T. $\Delta(T)$ follows a BCS-like temperature dependence (black curve) with $\Delta(0) \approx 0.25$ meV.

Once the emergence of superconductivity in W-doped $TaSe_2$ monolayers is established, we further investigate its evolution with W concentration, which is linearly proportional to the electron doping. We have studied 22 samples with different δ to cover the the range $0 < \delta < 0.07$. For each sample, we measure both the T and B dependence of the low-lying electronic structure, as previously described (Fig. 2). Figure 3 summarizes the evolution of the SC gap, the upper critical field (B_{C_2}) and T_C as a function of δ. The plotted values represent averaged values among all the
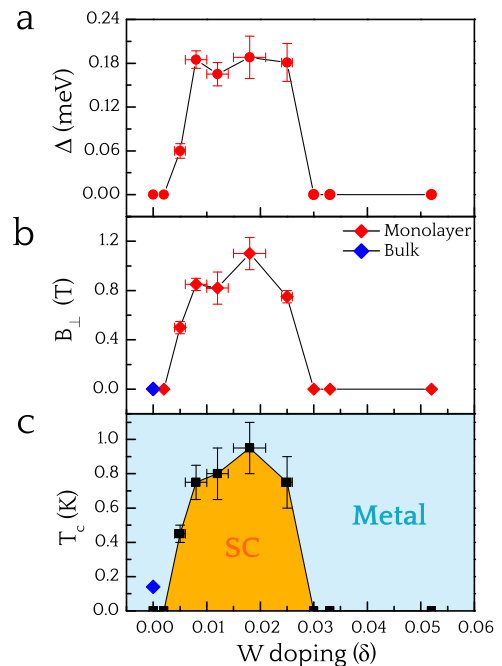

Fig. 3 Superconducting dome with electron (W) doping level. SC gap in **a**, upper critical field in **b**, and critical temperature in **c** as a function of W doping. All the values correspond to averaged values over the regions studied for a given δ. The error bars show the standard error of the mean.
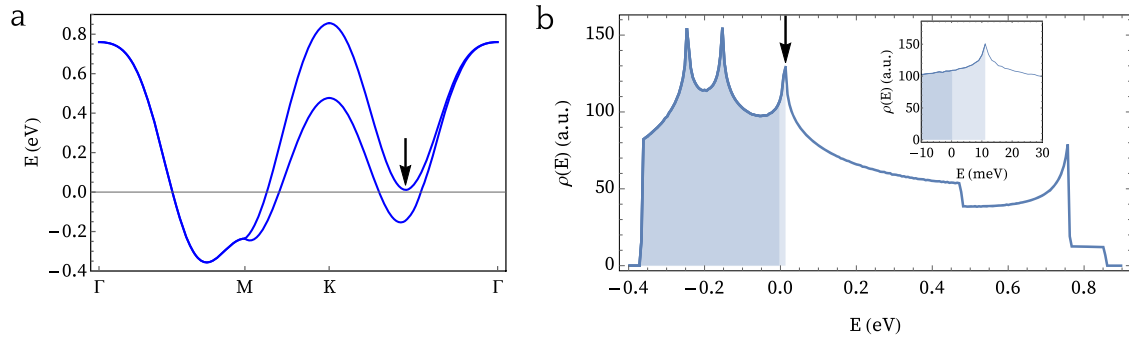
Fig. 4   Tight-binding model for TaSe$_2$. a Band structure. The vHs near E_F is marked with an arrow. **b** Calculated DOS with occupied states in dark blue. The amount of carriers needed to reach the vHs (light blue area) corresponds to $\delta = 0.02$.
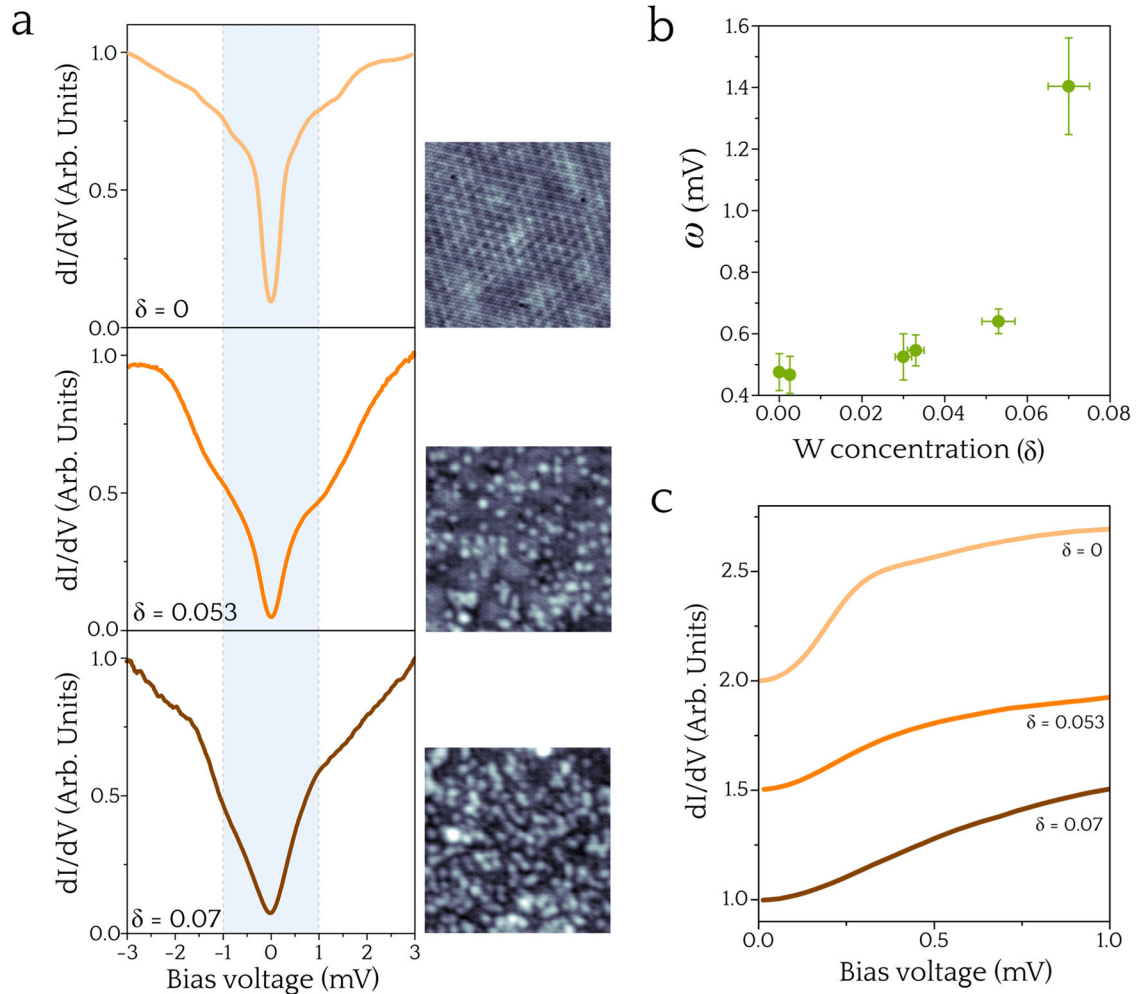

Fig. 5   Development of a disorder-induced Coulomb gap. a DOS evolution of the dip in Ta$_{1-\delta}$W$_\delta$Se$_2$ monolayer with δ. The STM images on the right show the corresponding morphology of the layer. **b** Width vs. δ in the non-superconducting regime. The error bars show the standard error of the mean. **c** Zoom-in of the dI/dV spectra shown in **a** illustrating the evolution of the differential conductance towards linearity at high disorder.

regions studied for each δ (see Supplementary Information). As seen, a superconducting dome spanning $0.003 < \delta < 0.03$ is found with a maximal $T_C \approx 0.9$ K for $\delta = 0.018$. Superconductivity develops for W concentrations as dilute as 0.5% ($\delta = 0.005$). This phase diagram reveals two additional interesting features. First, the superconducting state in the monolayer is significantly more

robust against $B_\perp$ with upper critical fields as large as $B_{C_2} \approx 1.1$ T with respect to the bulk, where B_{C_2} is in the mT range. Second, at the optimum W concentration for superconductivity, the SC gap reaches a value of $\Delta_{BCS} \approx 0.18$ meV, which leads to a lower bound for the ratio $2\Delta(0)/k_B T_C \geq 4.6$, a value significantly larger than the predicted by the BCS theory (3.53). This indicates that the pair-

coupling interaction is strong in the W-doped $TaSe_2$ monolayer. This enhanced value is nearly coincident with that of single-layer $NbSe_2$ ($\Delta(0) = 0.4$ meV, $T_C \approx 2$ K). Lastly, the Ginzburg–Landau coherence length estimated for this 2D alloy at optimum doping is $\xi_{GL}(T = 0$ K$) = 13.8$ nm, also very close to that for single-layer $NbSe_2$ (≈ 18 nm)[29,30].

Next, we discuss the origin of the superconductivity in electron-doped $TaSe_2$. The band structure of monolayer $TaSe_2$ has a saddle point near the E_F, around mid-way in the Γ-K direction, which leads to a logarithmic divergence in the DOS known as a van Hove singularity. SOC splits this vHs by about 0.23 eV according to DFT calculations[26–28], resulting in one peak slightly above E_F and one below it. This is also supported by ARPES experiments, which observe only one band along Γ-K[25]. As we dope electrons in $Ta_{1-\delta}W_\delta Se_2$ by increasing δ, E_F is tuned through the vHs, where superconductivity should be enhanced due to the increased DOS. This is therefore a natural explanation for the observed emergence of the super-conducting dome, similar to those found in 3D materials where the vHs is tuned by chemical doping[31] or strain[32].

To estimate the amount of W needed to reach the vHs, an accurate calculation of the DOS, the vHs and E_F positions is required. Since this value is not accurately reported in the literature, we use a tight-binding model with hoppings up to 5 nearest neighbors and SOC, chosen to reproduce the main features of the DFT bands of refs. [26–28]. The resulting band structure and corresponding DOS are shown in Fig. 4. The distance from E_F to the upper vHs peak is taken to be 5% of the vHs SOC splitting, which is within the values inferred from refs. [26–28]. This model is then used to compute the amount of electron doping needed to reach the vHs peak, which we obtain to be 0.015 electron/cell. This corresponds to a value of $\delta = 0.02$, in agreement with the dome maximum location.

Coulomb glass phase

A remaining question is the origin of the dip at E_F intrinsically present in pristine and W-doped $TaSe_2$. To gain knowledge here, we have analyzed the DOS within ± 1 mV for non-superconducting samples. Figure 5a shows three typical dI/dV spectra for different W concentrations. The dip within ± 1 mV shows a gradual increase of its width with δ accompanied by a change in shape. In particular, ω shows a non-linear increase with W concentration (plot in Fig. 5b, where ω represents the averaged ω over several different regions and/or samples). Furthermore, the shape of the dip evolves qualitatively towards a linear shape with W concentration (Fig. 5c).

At $\delta = 0$, a plausible origin for this intrinsic dip could be a CDW-induced partial gap within the main CDW gap (see Supplementary Information). However, the doping dependence of the dip would not conform to a CDW origin because chemical doping introduces disorder scattering, which would tend to suppress the CDW. Since disorder is present even in the undoped samples, we rather surmise that the dip is a disorder effect: the combination of small disorder and Coulomb interactions leads to a logarithmic dip of the DOS near E_F[33,34] (see fit in Fig. 1d). When disorder is further increased by doping, in 2D this dip evolves into power-law known as Coulomb gap, which widens with disorder. While the power is often quoted to be linear, numerical studies often deviate from this value[35,36]. Nevertheless, these observations are consistent with the emergence of a Coulomb gap driven by disorder. Since disorder is not expected to affect superconductivity due to Anderson's theorem, our global picture of $Ta_{1-\delta}W_\delta Se_2$ is that W substitution generates superconductivity as the nominal DOS is tuned through the vHs, while also increasing disorder so that a Coulomb gap develops at larger disorder strengths.

DISCUSSION

In summary, we prove the existence of superconductivity in a 2D metal with strong SOC where the Fermi surface is tuned at a saddle point in the band structure. Superconductors with such a band structure are candidates to host chiral/helical superconductivity and magnetic orders[37–41], and few of them have been identified in nature[42,43]. Our results open the doors to further experimental investigation in this type of alloys in search for signatures of topological superconductivity.

Lastly, the absence of superconductivity in a nearly isolated high-quality monolayer of $TaSe_2$ changes the picture of dimensionality effects on superconductivity in TMDs and calls for further theoretical efforts. Furthermore, our work highlights TMD alloys as ideal playgrounds for the study of a variety of disorder-driven electronic phase transitions in purely 2D systems, which have remained largely unexplored due to the lack of suitable platforms.

METHODS

Sample growth

Single-layer $Ta_{1-\delta}W_\delta Se_2$ samples ($0 < \delta < 0.07$) were grown on BLG/SiC(0001) substrates. The details for preparing BLG on SiC(0001) can be found in ref. [24]. For the growth of the TMD layer we co-evaporated high-purity Ta (99.95%), W (99.99%) and Se (99.999%) in our home-made molecular beam epitaxy (MBE) system under base pressure of ~5.0 × 10^{-10} mbar. The flux ratio between transition metals (Ta and W) and Se is 1:30. During the growth, the temperature of BLG/SiC(0001) substrates were maintained at 570°C and the growth rate was ~2.5 hours/monolayer. The flux of Ta was kept constant and the flux of W can be proportionally changed to control the stoichiometry δ. After the growth of the monolayer alloys, the samples were kept annealed in Se environment for 2 minutes, and then immediately cooled down to room temperature. In situ RHEED was used for monitoring the growth process. After the growth, a Se capping layer with a thickness of ~10 nm was deposited on the surface to protect the film from contamination during transport through air to the UHV-STM chamber. The Se capping layer was subsequently removed in the UHV-STM by annealing the sample at ~300 °C for 40 minutes prior to the STM measurements.

STM/STS measurements and energy resolution at 0.34 K

STM/STS data were acquired in a commercial UHV-STM system (Unisoku, USM-1300) operated at temperatures between 0.34 K and 4.2 K. This system is equipped with out-of-plane magnetic fields up to 11 T. For these experiments we used Pt/Ir tips previously calibrated on Cu(111) to avoid tip artifacts. The typical lock-in a.c. modulation parameters for low- and large-bias STS were ~30 μV (833 Hz) and ~5 mV (833 Hz), respectively. The dI/dV spectra shown in this work are averaged spectra from spatial grids (6 × 6 points) in regions of 10 × 10nm^2. The WSxM software were used for analysis and rendering our STM/STS data[44].

Since the superconducting gap structure in type-II super-conductors becomes spatially dependent in the presence of a $B_\perp$-field, we probed the $B_\perp$-field dependence of the DOS near E_F by carrying out nm-sized grid dI/dV spectroscopy in several locations of each sample for a given δ. The gradual weakening of the dip feature was always found in the $0.003 < \delta < 0.03$ range, where superconductivity develops (summarized in the Supplementary Fig. 5).

The energy resolution of our dI/dV measurements (dI/dV ∝ LDOS) at the lowest possible operational temperature of 0.34 K has been verified by measuring Josephson supercurrents in the two-band superconductor bulk Pb(111) with a superconducting Pb tip, which reveals a broadening of Γ ~105 ± 10 μV (see Supplementary Information). This broadening is mostly caused by the thermal broadening at $T = 0.34$ K ($\Gamma_{th} = 3.5 \cdot k_B T \approx 100$ μeV)

and, therefore, implies that the energy resolution is mostly limited by the base temperature of the instrument.

REFERENCES
1. Xi, X. et al. Ising pairing in superconducting NbSe$_2$ atomic layers. *Nat. Phys.* **12**, 139 (2016).
2. Sohn, E. et al. An unusual continuous paramagnetic-limited superconducting phase transition in 2D NbSe$_2$. *Nat. Mater.* **17**, 504 (2018).
3. Hamill, A. et al. Two-fold symmetric superconductivity in few-layer NbSe$_2$. *Nat. Phys.* **17**, 949 (2021).
4. Cho, C. et al. Nodal and nematic superconducting phases in NbSe$_2$ monolayers from competing superconducting channels. *Phys. Rev. Lett.* **129**, 087002 (2022).
5. Wan, W. et al. Observation of superconducting collective modes from competing pairing instabilities in single-layer NbSe$_2$. *Adv. Mater.* **34**, 2206078 (2022).
6. Cao, Y. et al. Quality heterostructures from two-dimensional crystals unstable in air by their assembly in inert atmosphere. *Nano Lett.* **15**, 4914 (2015).
7. Ugeda, M. M. et al. Characterization of collective ground states in single-layer NbSe$_2$. *Nat. Phys.* **12**, 92–96 (2016).
8. Zhao, K. et al. Disorder-induced multifractal superconductivity in monolayer niobium dichalcogenides. *Nat. Phys.* **15**, 904 (2019).
9. Galvis, J. A. et al. Scanning tunneling measurements of layers of superconducting 2H-TaSe$_2$: evidence for a zero-bias anomaly in single layers. *Phys. Rev. B* **87**, 094502 (2013).
10. Wu, Y. et al. Dimensional reduction and ionic gating induced enhancement of superconductivity in atomically thin crystals of 2H-TaSe$_2$. *Nanotechnology* **30**, 035702 (2018).
11. Navarro-Moratalla, E. et al. Enhanced superconductivity in atomically thin TaS$_2$. *Nat. Commun.* **7**, 11043 (2016).
12. Yang, Y. et al. Enhanced superconductivity upon weakening of charge density wave transport in 2H-TaS$_2$ in the two-dimensional limit. *Phys. Rev. B* **98**, 35203 (2018).
13. Peng, J. et al. Disorder Enhanced Superconductivity toward TaS$_2$ Monolayer. *ACS Nano* **12**, 24 (2018).
14. Ye, J. T. et al. Superconducting dome in a gate-tuned band insulator. *Science* **338**, 1193 (2012).
15. Li, L. J. et al. Controlling many-body states by the electric-field effect in a two-dimensional material. *Nature* **529**, 185–189 (2016).
16. Xi, X., Berger, H., Forró, L., Shan, J. & Mak, K. F. Gate tuning of electronic phase transitions in two-dimensional NbSe$_2$. *Phys. Rev. Lett.* **117**, 106801 (2016).
17. Li, P. et al. Phase transition and superconductivity enhancement in Se-substituted MoTe$_2$ thin films. *Adv. Mater.* **31**, 1904641 (2019).
18. Wang, S. et al. Phase-dependent band gap engineering in alloys of metal-semiconductor transition metal dichalcogenides. *Adv. Funct. Mater.* **30**, 2004912 (2020).
19. Gao, J. et al. Transition-metal substitution doping in synthetic atomically thin semiconductors. *Adv. Mater.* **28**, 9735–9743 (2016).
20. Gao, H. et al. Tuning electrical conductance of MoS$_2$ monolayers through substitutional doping. *Nano Lett.* **20**, 4095–4101 (2020).
21. Suh, J. et al. Doping against the native propensity of MoS$_2$: degenerate hole doping by cation substitution. *Nano Lett.* **14**, 6976–6982 (2014).
22. Zhang, T. et al. Universal in situ substitutional doping of transition metal dichalcogenides by liquid-phase precursor-assisted synthesis. *ACS Nano* **14**, 4326–4335 (2020).
23. Mallet, P. et al. Bound hole states associated to individual vanadium atoms incorporated into monolayer WSe$_2$. *Phys. Rev. Lett.* **125**, 036802 (2020).
24. Dreher, P. et al. Proximity effects on the charge density wave order and superconductivity in single-layer NbSe$_2$. *ACS Nano* **15**, 19430–19438 (2021).
25. Ryu, H. et al. Persistent charge-density-wave order in single-layer TaSe$_2$. *Nano Lett.* **18**, 689–694 (2018).
26. Ge, Y. & Liu, A. Y. Effect of dimensionality and spin-orbit coupling on charge-density-wave transition in 2H-TaSe$_2$. *Phys. Rev. B* **86**, 104101 (2012).
27. Yan, J. A., Dela Cruz, M. A., Cook, B. & Varga, K. Structural, electronic and vibrational properties of few-layer 2H- and 1T-TaSe$_2$. *Sci. Rep.* **5**, 1–13 (2015).
28. Lian, C. S. et al. Coexistence of superconductivity with enhanced charge density wave order in the two-dimensional limit of TaSe$_2$. *J. Phys. Chem. Lett.* **10**, 4076–4081 (2019).
29. Wang, H. et al. High-quality monolayer superconductor NbSe$_2$ grown by chemical vapour deposition. *Nat. Commun.* **8**, 394 (2017).
30. Xing, Y. et al. Ising superconductivity and quantum phase transition in macro-size monolayer NbSe$_2$. *Nano Lett.* **17**, 6802–6807 (2017).
31. Chikina, A. et al. Turning charge-density waves into Cooper pairs. *npj Quantum Mater.* **5**, 1–5 (2020).
32. Sunko, V. et al. Direct observation of a uniaxial stress-driven Lifshitz transition in Sr$_2$RuO$_4$. *npj Quantum Mater.* **4**, 1–7 (2019).
33. Kopietz, P. Coulomb gap in the density of states of disordered metals in two dimensions. *Phys. Rev. Lett.* **81**, 2120 (1998).
34. Butko, V. Y. U., DiTusa, J. F. & Adams, P. W. Coulomb gap: how a metal film becomes an insulator. *Phys. Rev. Lett.* **84**, 1543 (2000).
35. Möbius, A., Richter, M. & Drittler, B. Coulomb gap in two- and three-dimensional systems: Simulation results for large samples. *Phys. Rev. B* **45**, 11568 (1992).
36. Sarvestani, M., Schreiber, M. & Vojta, T. Coulomb gap at finite temperatures. *Phys. Rev. B* **52**, R3820 (1995).
37. Qin, W., Li, L. & Zhang, Z. Chiral topological superconductivity arising from the interplay of geometric phase and electron correlation. *Nat. Phys.* **15**, 796–802 (2019).
38. Huang, J. Q., Hsu, C. H., Lin, H., Yao, D. X. & Tsai, W. F. Chiral p-wave superconductivity in Sb(111) thin films close to Van Hove singularities. *Phys. Rev. B* **93**, 155108 (2016).
39. González, J., Guinea, F. & Vozmediano, M. A. H. Kinematics of electrons near a van Hove singularity. *Phys. Rev. Lett.* **84**, 4930 (2000).
40. Wang, Y., Liu, J. G., Wang, W. S. & Wang, Q. H. Electronic order near the type-II van Hove singularity in BC$_3$. *Phys. Rev. B* **97**, 174513 (2018).
41. Nandkishore, R., Levitov, L. S. & Chubukov, A. V. Chiral superconductivity from repulsive interactions in doped graphene. *Nat. Phys.* **8**, 158–163 (2012).
42. Wang, D. et al. Evidence for Majorana bound states in an iron-based superconductor. *Science* **362**, 333–335 (2018).
43. Zhang, P. et al. Observation of topological superconductivity on the surface of an iron-based superconductor. *Science* **360**, 182–186 (2018).
44. Horcas, I. et al. WSXM: A software for scanning probe microscopy and a tool for nanotechnology. *Rev. Sci. Instrum.* **78**, 013705 (2007).

AUTHOR CONTRIBUTIONS
W.W. and M.M.U. conceived the experiment. W.W. carried out the MBE growth, the morphology characterization of the samples with the help of R.H. and P.D. W.W. measured and analyzed the STM/STS data with the help of M.M.U. M.M.U. supervised the project. F.d.J. provided the theoretical support. M.M.U. and F.d.J. wrote the paper with help from the rest of the authors. All authors contributed to the scientific discussion and manuscript revisions.

COMPETING INTERESTS
The authors declare no competing interests.

ADDITIONAL INFORMATION
Supplementary information The online version contains supplementary material available at https://doi.org/10.1038/s41699-023-00401-4.

Correspondence and requests for materials should be addressed to Miguel M. Ugeda.

Reprints and permission information is available at http://www.nature.com/reprints

Publisher's note Springer Nature remains neutral with regard to jurisdictional claims in published maps and institutional affiliations.